Arabian Journal of Chemistry (2019) **12**, 559–572

King Saud University

Arabian Journal of Chemistry

www.ksu.edu.sa
www.sciencedirect.com

ORIGINAL ARTICLE

Porous multifunctional fluoropolymer composite foams prepared via humic acid modified Fe_3O_4 nanoparticles stabilized Pickering high internal phase emulsion using cationic fluorosurfactant as co-stabilizer

Umair Azhar, Chenxi Huyan, Xiaozheng Wan, Chuanyong Zong, Anhou Xu, Jitao Liu, Jiachen Ma, Shuxiang Zhang *, Bing Geng *

Shandong Provincial Key Laboratory of Fluorine Chemistry and Chemical Materials, School of Chemistry and Chemical Engineering, Shandong Engineering Research Center for Fluorinated Materials, University of Jinan, Jinan 250022, China

Received 24 January 2018; accepted 3 April 2018
Available online 14 April 2018

KEYWORDS

HIPE;
Co-stabilization;
Fluoropolymer;
Adsorption;
Hydrophobic;
Functional porous polymer

Abstract Fluoropolymers are very important owing to their excellent application performances, especially in extreme conditions. On the other hand, the preparation of porous fluoropolymers is a difficult task due to unavailability of suitable surfactants as well as tedious synthesis steps. Here we prepared multifunctional porous fluoropolymer composite foams with a simple process of "high internal phase emulsion (HIPE)" by using humic acid modified iron oxide nanoparticles (HA-Fe_3O_4 NPs) and cationic fluorosurfactant (CFS) (PDMAEMA-*b*-PHFBA) as co-stabilizer. The inclusion of HA-Fe_3O_4 NPs in the system made fluoro-HIPE more stable than the emulsion prepared using only CFS or other conventional stabilizers. Morphology of the prepared polyHIPE was easily controlled by altering the concentration of HA-Fe_3O_4 and/or CFS in the original formulation. Adjustment of the porous structure with open/close cells was performed and the average diameter of the pores tuned between 4.9 and 23 μm. With the increase in specific surface area by using nanoparticles (NPs) and CFS as co-surfactants, Pickering HIPE monoliths adsorbed double amount of oil compared to foams based solely on HIPE template. Multiple functional groups were bound onto Fe_3O_4

* Corresponding authors.
E-mail addresses: chm_zhangsx@ujn.edu.cn (S. Zhang), chm_gengb@ujn.edu.cn (B. Geng).
Peer review under responsibility of King Saud University.

Production and hosting by Elsevier

https://doi.org/10.1016/j.arabjc.2018.04.003

NPs through HA modification that made the fluoro-monolith capable of adsorbing dye, i.e. methylene blue, from water. A simple centrifugation enabled regeneration of the oil soaked foams and adsorption capacity was not decreased after 10 adsorption/regeneration cycles.

1. Introduction

In recent years, porous polymers have gained an increased level of research interest because of their high specific surface area (SSA), superb interconnectivity and well-defined porosity. These significant properties allow their use in enormous practical applications such as tissue engineering scaffolds (Dhandayuthapani et al., 2011; Jafari et al., 2017), reaction supports for catalysts (Debecker et al., 2015), separation membranes (Tebboth et al., 2014), oil adsorption (Wang et al., 2015), heavy metal ion collectors (Pan et al., 2016), responsive materials (Schacher et al., 2009) and so on (Kimmins and Cameron, 2011). There are a lot of ways by which porous polymers can be prepared for example direct templating (Lu and Schüth, 2006), block copolymer self-assembly (David and Olson, 2007), direct synthesis methodology (McKeown and Budd, 2010), high internal phase emulsion (HIPE) (Kimmins and Cameron, 2011), interfacial polymerization (Wenwen, 2010), and breath figures methodology (Chen et al., 2011), etc. (Wu et al., 2012). Among all processes, HIPE is easily controllable and flexible to fabricate macroporous materials with desired pore sizes and morphology. HIPEs are the system of highly viscous, paste-like emulsions in which major, "droplet" phase normally defined as occupying more than 74 wt%, is dispersed within minor, "continuous phase" (Cameron, 2005), whereas polyHIPEs are the porous emulsion templated polymers synthesized within HIPEs (Azhar et al., 2017a). Inside morphology of polyHIPE can be easily converted into open or closed cells. The closed cells porous structures are very attractive materials for applications such as thermal insulations and precursor of carbon materials, while highly interconnected porous polymer (open cells) foams are promising materials for catalysts supports, adsorption and separation applications (Sumirat et al., 2006; Fongang et al., 2015).

The monomers, based on hydrocarbons such as styrene, methacrylates and vinyl, are commonly used for polymerization to prepare polyHIPEs (Brun et al., 2011). With the replacement of hydrogen atoms by fluorine atoms, fluoropolymers exhibit superior physicochemical properties as compared to conventional polymers in many aspects, such as hydrophobicity, optical transparency, solvents compatibility, oxidative/chemical resistivity and environmental stability (Huang et al., 2005). For these substantial benefits, research on fluorinated oils, surfactants and block copolymers have gained tremendous focus of researchers in the field of emulsion polymerization (Ma et al., 2017; Azhar et al., 2017b; Xu et al., 2017). Until now, a limited number of studies have been conducted on the fluoro-HIPE system, mainly due to the difficulty in synthesis process and lack of compatible surfactants.

To attain stable HIPE, surfactants play a critical role in the dispersion of droplet phase within the continuous phase of HIPE and are the key factor to achieve polyHIPEs with adjustable morphology (Raffa et al., 2015). Stabilization of fluoro-HIPEs is a difficult task because many conventional surfactants like SPAN 80, CTAB and Tween 80 are unable to stabilize these kinds of emulsions (Azhar et al., 2017a, b; Wan et al., 2018). In our previous work, we prepared a very effective cationic fluorosurfactant (CFS) in order to stabilize the fluoro-HIPEs. High-performance fluoropolymer foams were synthesized after polymerization of those fluoro-emulsions (Azhar et al., 2017a). However, the surface areas and porosities were not high enough to get more advantages of their practical applications. Stability of fluoro-HIPE maintained solely by CFS also needed to improve because of the CFS's limited stability effect. To solve the above issues, we got some clues from Pickering emulsion for utilizing nanoparticles to stabilize the emulsions (Vilchez et al., 2014).

Solid nanoparticles just like silica, titania, hydroxyapatite, polymeric nanoparticles, carbon nanotubes and magnetite can adsorb at interfaces and accordingly stabilize emulsions. Such emulsions are known as Pickering emulsions (Aveyard et al., 2003; Guo et al., 2017). Pickering emulsions show good stability performances due to the irreversible NPs layer at the oil/water interface, which hinders the droplet coalescence (Toledo and Urbano, 2016). Moreover, by attaching various functional groups on nanoparticles (NPs) and then incorporating these NPs into the polymer matrix, functional composites can be achieved (Mert et al., 2013). Based on the advantages of Pickering emulsion, researchers have designed a very handy strategy to obtain highly porous and interconnected polyHIPEs by using a co-stabilization mechanism, in which nanoparticles and surfactant molecules can be used simultaneously (Hongyun, 2015; Yin et al., 2014a). Whereas water-oil interfacial tension is reduced by amphiphilic surfactant, while NPs form rigid shells that surround the internal phase and prohibit coalescence (Yin et al., 2014b), and it ultimately increases emulsion stability.

The use of magnetic nanoparticles cuts down overall operating and capital costs (Mert et al., 2013). Also, magnetic polyHIPEs with conjoined benefits of polymers and magnetic nanoparticles have received huge attention in the fields of medicine and pollution control (Kawaguchi, 2000; Ruiz-Hernández et al., 2008; Wu et al., 2017). One of the most attractive advantages of magnetic polyHIPEs is their quick and facile separation with the applied external magnetic field. Humic acid (HA) is an abundant organic material in aqueous systems, which demonstrates high reaction activity because of aromatic hydrocarbons and a lot of carboxyl, phenolic hydroxyl, carbonyl, methoxyl, alcoholic hydroxyl, ether and amino groups in the skeleton (Xiaojuan, 2006). Binding HA to metal oxides influences sorption behavior of both HA and metal oxides. This alters the surface properties of particles because adsorption of HA results in the polyanionic organic coating on metal oxides. Though HA has a predominant affinity with most of the organic compounds (Xiaojuan, 2006), but separation of HA from the water is a big problem. So it is a good tentative idea

to bind HA modified iron oxide nanoparticles into the polymer matrix to deal with this bottle neck (Mert et al., 2013).

In this work, for the first time, humic acid modified Fe_3O_4 NPs were used to enhance the properties of fluoropolymer composite foams. The fluoroHIPEs were co-stabilized by HA-Fe_3O_4 and CFS. Stability of these fluoroHIPEs was proved to be significantly higher compared to the emulsions solely stabilized by CFS. Effect of NPs and CFS on morphology of resulting foams was investigated. Moreover, Oil and dye adsorption capacities along with hydrophobicity, magnetism and recyclability of fluoropolymer composite foams were studied.

2. Experimental

2.1. Materials

Humic acid sodium salt (technical grade) was purchased from Sigma-Aldrich. 2-(dimethylamino)ethyl methacrylate (DMAEMA, 99%) and passed through basic alumina column to remove inhibitor. Iron(II) chloride tetrahydrate ($FeCl_2{\cdot}4H_2O$) were purchased from Shanghai Macklin Biochemical Co. Ltd. Hexafluorobutyl acrylate (HFBA) was supplied by Fluorine Silicon Chemical Company and passed through alkaline alumina column as well to get rid of any inhibitor prior to use. Iron chloride hexahydrate ($FeCl_3{\cdot}6H_2O$), dichloromethane (DCM) and divinylbenzene (DVB, 80%) were purchased from Aladdin. Methylene Blue dye (MB), sudan III dye, dioxane, ammonia solution (NH_3; 25–28%), cetyltrimethylammonium bromide (CTAB), Tween 80 and tetrahydrofuran (THF) were bought from Sinopharm Chemical Reagent Co. Ltd. 2,2′-azobisisobutyronitrile (AIBN) was purchased from Lingfeng Chemical Reagent Co. Ltd. n-Hexane (>97%) was provided by Tianjin Fuyu Chemical Company. Calcium carbonate dihydrated ($CaCl_2{\cdot}2H_2O$) was supplied by Shanghai Zhanyun Chemical Co. Ltd. Deionized water (DI) was used throughout the experiments. Cumyl dithiobenzoate (CDB-RAFT agent) was synthesized by the procedure given elsewhere (Yang Liu, 2005).

2.2. Synthesis of cationic fluorosurfactant Poly(2-dimethylamino)ethyl methacrylate-b-Poly(hexafluorobutyl acrylate)

Macro-chain transfer agent, i.e. poly(2-dimethylamino)ethyl methacrylate (PDMAEMA), was first prepared as previously reported (Azhar et al., 2017a). CFS was prepared as follows, hexafluorobutyl acrylate (HFBA; 2.8 g; 11.86 mmol), 2,2′-azo bis-isobutyronitrile (AIBN; 0.0284 g, 0.17 mmol), macro-CTA (PDMAEMA; 4 g; 0.62 mmol) macro-CTA/AIBN molar ratio = 3.65 were dissolved in (1,4-dioxane; 11.9141 g) by using 50 mL round bottom flask. The reaction mixture was sealed and purged with nitrogen gas to completely eradicate oxygen from the flask. The oxygen free solution was then placed in a preheated oil bath at 70 °C for 13 h with magnetic stirring. Then the reaction was quenched by placing the vessel in ice water. Finally, excess cold petroleum ether was used to precipitate and purify the resulting di-block PDMAEMA-*b*-PHFBA followed by drying at room temperature under vacuum for 24 h.

2.3. Preparation of bare Fe_3O_4 and HA-Fe_3O_4 nanoparticles

Bare and humic acid modified iron oxide nanoparticles were prepared according to the published method (Jing-Fu, 2008). Typically; $FeCl_3{\cdot}6H_2O$ (5.96 g) and $FeCl_2{\cdot}4H_2O$ (3.08 g) were dissolved in 100 mL of water in a 250 mL round-bottom flask equipped with a reflux condenser. The iron solution was heated to 90 °C and mechanically stirred throughout the reaction process. 10 mL of 25–28% ammonia solution and 50 mL of 1% humic acid solution (for HA-Fe_3O_4 synthesis) were rapidly and sequentially added to the mixture. The reaction mixture was further allowed to stir for 30 min at 90 °C. Finally, the solid product was washed with water several times and dried in a vacuum oven at 40 °C. The dried particles were stored in a vacuum desiccator to avoid moisture adsorption.

2.4. Preparation and polymerization of magnetic polyHIPEs

A typical water in oil (W/O) HIPE with 80.4 wt% water as internal phase was prepared as follows (Table 1; sample 3). The cationic fluorosurfactant (PDMAEMA-*b*-PHFBA; 0.3948 g) was dissolved in hexafluorobutyl acrylate (HFBA; 3.5561 g) and divinylbenzene (DVB; 0.3951 g). Then 2,2′-azo bis-isobutyronitrile (AIBN; 0.0395 g) and HA-coated iron oxide nanoparticles (HA-Fe_3O_4; 0.2193 g) were added. The mixture was sonicated for 30 min to evenly disperse the nanoparticles. After that, the mixture was taken in a three-necked flask and an aqueous solution of 0.2 M calcium chloride dihydrated ($CaCl_2{\cdot}2H_2O$; 18 g) was added drop wise with continuous mechanical stirring (450 RPM). The mixture was further allowed to agitate for 30 min at the same speed. Then the prepared HIPE was taken into the centrifugal tube and set in an oven at 60 °C for 24 h to polymerize. The obtained monoliths were purified by Soxhlet extraction with absolute ethanol to remove unreacted monomers and other impurities followed by drying at 60 °C for 24 h to get porous polyHIPE. Similar systems of fluoro-emulsions were prepared by varying amount of CFS and nanoparticles to see their effect on the final morphology of the product. By keeping magnetite concentration same at 4 wt% with respect to continuous phase, CFS concentrations were varied (Table 1; samples 1–4). Amount of magnetite nanoparticles were altered in (Table 1; samples 5–7) while keeping CFS concentration constant at 8 wt%. Another polyHIPE was prepared with 6 wt% CFS without HA-Fe_3O_4 nanoparticles (Table 1; sample 8) to analyze magnetization and emulsion stability. Conventional surfactants Tween 80 (Table 1; Sample 9) and CTAB (Table 1; Sample 10) were employed with HA-Fe_3O_4 nanoparticles to see their effect on HIPE.

3. Characterization

3.1. ^1H NMR spectroscopy

^1H NMR spectra of PDMAEMA (first block) and PDMAEMA-*b*-PHFBA (CFS) were recorded using Bruker Advance III 400 MHz nuclear magnetic resonance spectrometer at room temperature. Deuterated DMSO was used as a solvent to dissolve samples in ^1H NMR tubes before spectroscopy.

Table 1 Morphology, formulation, porosity, specific surface area, emulsion stability (± values represent standard deviation).

Sample[a]	HA-Fe_3O_4 (wt%)[b]	Cationic fluorosurfactant (wt%)[b]	Conventional surfactant (wt%)[b]	AIBN (wt%)[b]	DVB/HFBA mass ratio	Morphology[c]	Specific surface area (m^2/g)[d]	Porosity (%)[e]	HIPE stability (h)
1	4	3	0	1	0.1	Open	24.5 ± 2.2	77.16	> 48
2	4	6	0	1	0.1	Open	27 ± 2.3	79.14	> 60
3	4	9	0	1	0.1	Open	29.8 ± 2.5	81.9	> 96
4	4	12	0	1	0.1	Irregular	–	–	> 96
5	2	8	0	1	0.1	Open	25.12 ± 1.6	76.1	> 72
6	7	8	0	1	0.1	Open	24.7 ± 2.4	77.1	> 96
7	10	8	0	1	0.1	Closed	24 ± 0.8	76.8	> 96
8[f]	0	6	0	1	0.1	Open	15.4 ± 2	77.8	< 72
9[g]	4	0	8	1	0.1	–	–	–	NE
10[h]	4	0	8	1	0.1	–	–	–	NE

[a] The dispersed phase volume of all HIPEs is 80 wt%.
[b] With respect to the continuous phase.
[c] SEM images.
[d] BET.
[e] Liquid displacement test (Ruiyun, 1999).
[f] Without nanoparticles.
[g] Tween 80 as commercial surfactant.
[h] CTAB as commercial surfactant, NE stands for no emulsion.

3.2. Scanning electron microscopy (SEM) and energy Dispersive X-ray spectroscopy (EDXS)

The structure of porous fluoropolymer was studied with scanning electron microscope (SEM, S-2500, Hitachi Seiki Ltd., Japan). The accelerating voltage was 8 kV. Before SEM approximately 0.5 cm^3 of each fractured surface sample was fixed on carbon tape attached to aluminum stub. The sample was sputtered with gold at 20 mA for 80 s by using (Scan Coat Six SEM Sputter Coater, Edwards, Ltd., Crawley, United Kingdom) in order to ensure good electrical conductivity. Images of the surfaces were taken from top, middle and bottom portions to account for variations in pore morphology because of sedimentation and coalescence. Dimensions of pores and pore throats were analyzed using SEM images with the help of Nano Measurer 1.2 software. SEM was linked with OXFORD X-MAX-50 INCA to obtain local atomic concentration of various elements in magnetic polyHIPEs through EDXS.

3.2. Size exclusion chromatography

Dispersity (Đ) and number average molecular weight of macro chain transfer agent (PDMAEMA) and di-block copolymer (PDMAEMA-*b*-PHFBA) were characterized by gel permeation chromatography (GPC). All measurements were performed at 25 °C by using "Waters 1500" that consisted of Refractive index detector and HPLC pump. THF with a flow rate of 1 mL/min was used as mobile phase. 25 mg of each sample was dissolved in THF and injected at a concentration of 3 mL/L after filtration through 0.45 μm size membrane.

3.3. Specific surface area and porosity

Specific surface areas (SSA) of magnetic fluoropolymers were determined by Brunaur-Emmett-Teller (BET) model surface area analyzer Micromeritics TriStar II 3020 using nitrogen adsorption isotherm. Prior to gas adsorption, contaminants were eliminated via a "Degassing" step, where approximately 200 mg of each sample was heated at 120 °C for 12 h in glass sample cells. Porosity of the material was calculated by liquid displacement test (Ruiyun, 1999).

3.4. Hydrophobicity measurement

Hydrophobicity of magnetic porous fluoropolymer foams was measured by a contact angle instrument OCA drop shape analyzer (Data Physics Co., Germany) at room temperature. Images of the contact angle were taken after 2 min of water droplet stay on the polymer surface.

3.5. Oil adsorption test

0.2 g (approximately 20 mm in diameter and 12 mm in height) of polyHIPE foam in cylindrical shape was placed into the oil/water mixture (oil floated on the surface of water). A hand-held magnet was used to move and take out the magnetic monolith from water surface after achieving oil adsorption saturation. Oil intake capacity k was calculated by the following equation:

$$k = \frac{m_1 - m_0}{m_0} \quad (1)$$

where m_1 is the mass of the foam after oil adsorption and m_0 is the mass of foam before oil adsorption. Three replicates were performed for each polyHIPE sample.

3.6. Dye adsorption test

Macroporous magnetic monolith (0.2 g) was immersed in 25 mL of Methylene Blue solution (10 ppm). The dye solution with monolith was shacked with speed of 180 at 45 °C by using

a thermostatic shaker. The remaining concentration of MB in the solution was measured at various time intervals via a UV–vis spectrophotometer. The adsorption capacity q_t (mg/g) of functional polyHIPE at time t was determined by the given formula:

$$q_{t=\frac{(C_1-C_2)}{m}\times V} \quad (2)$$

where C_1 is the initial concentration of dye (mg/L); C_2 is the concentration of MB at time t (mg/L); V is the volume of the solution in liter (L), and m is the mass of the foam (g). The adsorption kinetics experiments on polyHIPEs without functional nanoparticles were also carried out for comparison under same conditions. Three replicates experimented for each sample.

3.7. Degree of openness calculation

The degree of openness of polyHIPEs was calculated by the relationship reported elsewhere (Pulko and Krajnc, 2012). The typical equation used for openness (O) is given below,

$$O = \frac{N.d^2}{4.D^2} \quad (3)$$

where N represents number of pore throats, d is average pore throats diameter and D is average pore diameter.

3.8. Optical microscopy

The shape and size of HIPE droplets were observed by Nikon Eclipse LV100POL, Japan optical microscope after dribbling emulsion droplet on glass slides. The samples for optical microscopy were analyzed immediately after preparation of the HIPE.

3.9. Fourier transform Infrared spectroscopy (FTIR)

Infrared spectra of magnetic polyHIPE, bare iron oxide nanoparticles (Fe_3O_4) and those modified with humic acid were recorded on NICOLET iS10, ThermoFisher SCIENTIFIC, USA. PolyHIPE was transformed into powder form before characterization. The wavenumber range was in between 250 and 2500 cm^{-1} with resolution of 4.1 cm^{-1}.

3.10. X-ray diffraction (XRD)

The X-ray powder diffraction analysis of bare and humic acid modified nanoparticles was performed on BRUKER D8 FOCUS. The sample was ground into fine powder form before XRD analysis. XRD peaks were analyzed using MDI Jade 6 software.

3.11. Vibrational sample magnetometery (VSM)

The magnetic properties of the polyHIPEs prepared with bare and humic acid modified Fe_3O_4 nanoparticles were observed by Quantum Design Vibrating Sample Magnetometer (VSM model 6000).

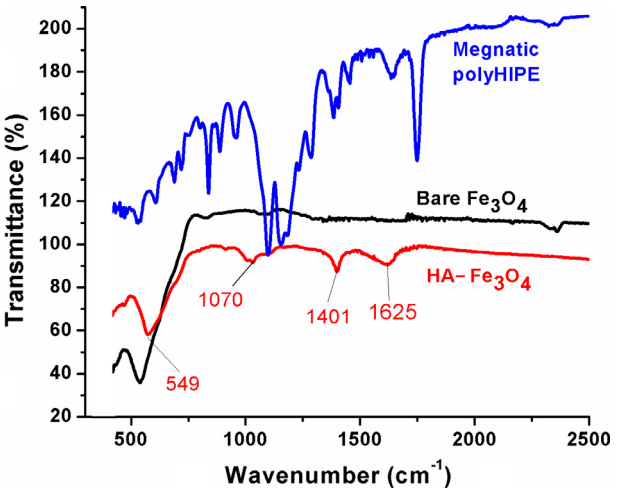

Fig. 1 FTIR spectra of bare Fe_3O_4, Humic acid coated Fe_3O_4 and magnetic polyHIPEs.

4. Results and discussions

4.1. Characterization of bare and HA-Fe_3O_4 nanoparticles

FTIR spectra of magnetic polyHIPE (sample 3), bare and humic acid coated nanoparticles are given in Fig. 1. From the spectroscopic study, it is clear that humic acid has been successfully coated on iron oxide nanoparticles. The characteristic peaks of iron oxide that contains only metal-oxygen band were observed at 549 cm^{-1} related to intrinsic stretching vibrations of metal at tetrahedral site (Fe—O). The band at 1401 cm^{-1} was due to CH_2 scissoring (Peng et al., 2012). The C—O stretches of COO^- were observed at 1070 cm^{-1}. C═O stretches of HA/Fe_3O_4 at 1625 cm^{-1} showed the interaction between FeO surface and carboxylate anion, as C═O stretches

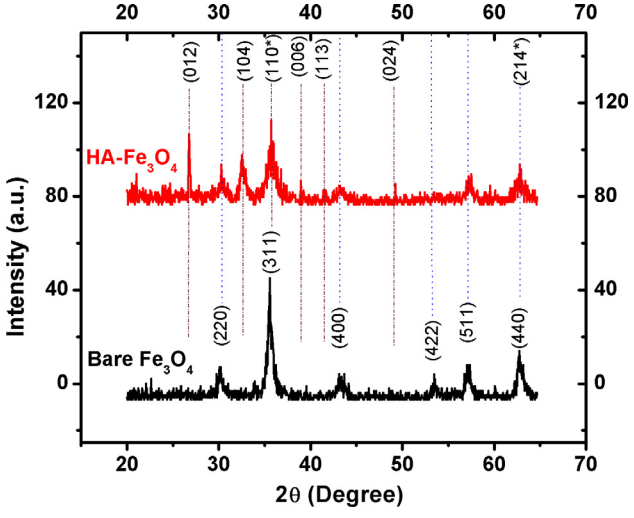

Fig. 2 XRD patterns of bare Fe_3O_4 and humic acid modified Fe_3O_4 nanoparticles.

in free carboxylic acid was above 1700 cm^{-1} (Wassana, 2007). For bare iron oxide nanoparticles, there were no C—O and C═O stretches observed, suggested the perfect binding of humic acid to Fe_3O_4. It is commonly believed that binding of humic acid to iron oxide surface is basically through ligand exchange (Baohua Gu et al., 1994).

Fig. 2 depicts X-ray diffractograms recorded for bare iron oxide and HA-coated iron oxide particles. The single phase spinal structure was confirmed as no extra peaks and unreacted constituents were observed. All XRD peaks were indexed by the cubic structure of iron oxide (JCPDS No. 99-101-2014), that confirmed a high phase purity of the product: (2 2 0), (3 1 1), (4 0 0), (4 2 2), (5 1 1) and (4 4 0) in the order of increasing diffraction angle. The resulting broad diffraction peaks had the small crystallite size. In order to determine the crystallite size of the product, the most intense peak of 311 was taken with the help of Scherrer formula and average crystallite size was found to be 14.33 nm. The X-ray diffraction pattern of HA-coated magnetite evidenced that the particles were almost in magnetite crystal phase while small amount of maghemite could be deduced from other peaks. The resulting peaks (0 1 2), (1 0 4), (1 1 0*), (0 0 6), (0 2 4), (1 1 3) and (2 1 4*) were indexed with maghemite (JCPDS No. 99-101-0140). By comparing the most intense peaks at (1 0 4) for maghemite and (3 1 1) for magnetite, it can be clearly seen that magnetite was dominant crystal structure. This can be elaborated by the surface treatment phenomena of HA-Fe_3O_4 magnetic nanoparticles. The surface of Fe_3O_4 can be oxidized to form Fe_2O_3 (oxygen-rich) structure as secondary crystal phase at the surface (Tian et al., 2011).

4.2. Characterization of cationic fluorosurfactant (CFS)

RAFT polymerization technique was employed to synthesize a copolymer Poly(2-dimethylamino)ethyl methacrylate-*b*-Poly (hexafluorobutyl acrylate) (PDMAEMA-*b*-PHFBA), which was named as a cationic fluorosurfactant. Cumyl dithiobenzoate (CDB) was used as a RAFT agent. Molecular weight and its distribution were confirmed by GPC. Only one single peak with a significant shift towards higher molecular weight confirmed the synthesis of a di-block copolymer (PDMAEMA-*b*-PHFBA) rather the mixture of homopolymers of both PDMAEMA and PHFBA (Fig. S1). Narrow dispersity (Đ; 1.25) and increased molecular weight (M_n; 8.2×10^3 g/mol) with respect to the macro chain transfer agent (Đ; 1.15, M_n; 6.5×10^3 g/mol) was the proof of excellent control of RAFT polymerization for di-block copolymer synthesis. The structure and composition of CFS were further investigated by ^{1}H NMR Fig. 3). The mean degree of polymerization of macro-CTA came out to be 51 by comparing the integrated signals to RAFT agent aromatic protons (7–7.8 ppm) with those assigned to two methylene protons of PDMAEMA at 3.9–4.19 ppm. The feature signals of 1st block PDMAEMA δ = 2.3 ($(CH_3)_2NCH_2CH_2$—) (f H), δ = 2.5 ($(CH_3)_2NCH_2CH_2$—) (e H), δ = 4.01 ($(CH_3)_2NCH_2CH2$—) (d H) and for PHFBA block δ = 6.01($CF_3CHFCF_2CH_2$—) (h H), δ = 4.54 ($CF_3CHFCF_2CH_2$—)(g H) were appeared in ^{1}H NMR spectrums (Azhar et al., 2017a). The degree of polymerization of the second block (PHFBA) was calculated to be 25.

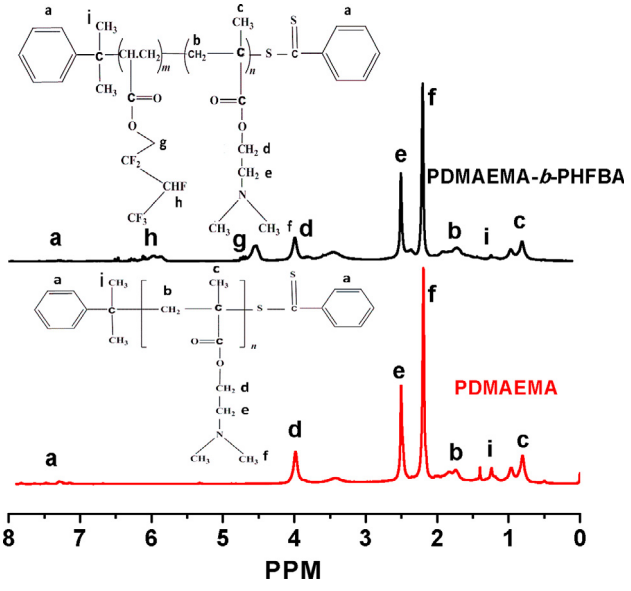

Fig. 3 ^{1}H NMR curves of PDMAEMA and PDMAEMA-*b*-PHFBA.

4.3. Optical microscopy, droplet size distribution and stability of HIPE

During HIPE preparation a significant amount of water (80 wt %) was dispersed in oil phase with co-existence of HA-Fe_3O_4 and cationic fluorosurfactant (PDMAEMA-*b*-PHFBA). Then free radical polymerization was adopted to polymerize the continuous phase of HFBA and DVB by using AIBN as an initiator, which resulted in solidification after reaction completion.

Water (dispersed phase) was then eliminated by action of drying to obtain extremely porous fluoropolymer monoliths. These polyHIPEs possessed relatively homogeneous and highly interconnected open structure which was similar to the microstructure of typical polyHIPEs (Silverstein, 2014). The fluoro-emulsions prepared in this study showed remarkable stability performances. Optical images and droplet size distribution curves of emulsion prepared by 9 wt% CFS with 4 wt% HA-Fe_3O_4, 6 wt% CFS with 4 wt% HA-Fe_3O_4 and 6 wt% CFS with no nanoparticles are presented in Fig. 4a–c. Stability of co-stabilized emulsion was found to be significantly higher than that of the emulsion prepared only by CFS. The reason to explain this difference in emulsion stabilities of both systems is that besides adsorption, the addition of emulsifiers (in mixed emulsifier-NPs system) can also take part in lowering the interfacial tension, thereby facilitating the emulsification and allowing simultaneous adsorption of both NPs and surfactant at the oil/water interface, thus imparting long-term emulsion stability (Pichot et al., 2010).

It is obvious from Fig. 4d that the average droplet sizes reduced in HIPEs stabilized by mixed CFS and HA-Fe_3O_4 emulsion systems, as compared to the emulsion stabilized solely by surfactant. The average droplet sizes of the emulsion prepared without nanoparticles (sample 8) were estimated to be 18–22.8 μm. On the other hand, droplet sizes were found to be in a range of 12–19 μm and 4.9–14 μm for sample 2 and sample 3, respectively. The decrease in average droplet sizes may be attributed to the stabilization mechanism of these mixed emulsifier systems. In which both CFS and NPs had

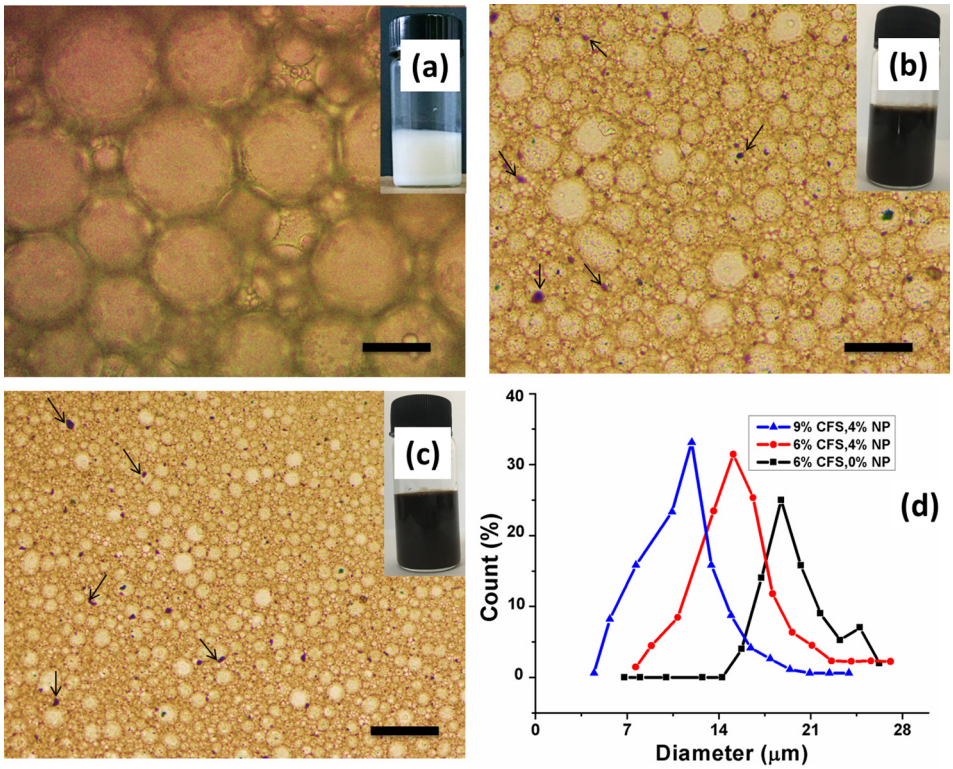

Fig. 4 Droplet size control and size distributions of HIPEs (co-stabilization process decreases droplet sizes) by optical microscope images: (a) sample 8, (b) sample 2, (c) sample 3, and (d) Droplet size distribution curves; (scale bar 20 μm).

specific functions. More specifically, the role of CFS was to initially "delay" the coalescence process and accelerate further droplet breakdowns during HIPE formation, by quickly covering the newly created oil/water interface and decreasing interfacial tension. This allowed HA-Fe_3O_4 nanoparticles to assemble at the interface and provided long-term stability to the magnetic HIPEs (Pichot et al., 2010). Some NPs aggregates were observed in the continuous phase of HIPEs, mostly between neighboring droplets (Fig. 4b,c) which indicated that the tiny particles were pulled out from the oil/water interface by CFS adsorption on the particle surface (small arrows in Fig. 4b,c). This finding of aggregated NPs is in agreement with

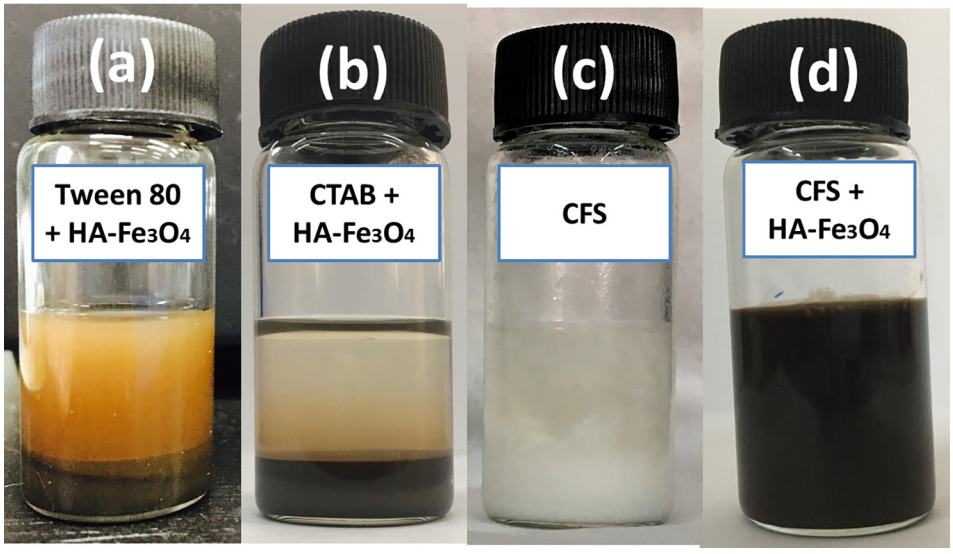

Fig. 5 Stabilities of fluoro-emulsions emulsified with different stabilizers: (a) sample 9 (image taken after 15 min), (b) sample 10 (image taken after 15 min), (c) sample 8 (image taken after 3 days), (d) sample 6 (image taken after 5 days).

the recent literature report about magnetite nanoparticles and highly concentrated Pickering emulsions (Vilchez et al., 2014). On the other hand, no nanoparticles agglomerates were seen in Fig. 4a as it was the emulsion solely stabilized by the surfactant (not with nanoparticles).

Commercial surfactants Tween 80 and CTAB were used one by one with HA-Fe_3O_4 nanoparticles to compare the stability of HIPE against CFS co-stabilized with magnetite emulsion (Fig. 5). It is clear from the digital images that conventional surfactants failed to give an emulsion. A clear bi-phase separation was observed in Fig. 5a, b. HIPE stabilized with only CFS was started phase separation after 3 days of emulsion preparation Fig. 5c, but HIPE co-stabilized by CFS and HA-Fe_3O_4 demonstrated viscous emulsions with obtrusive stability even after 5 days Fig. 5d). Hence by this way, our designed system of co-stabilized HIPEs was highly efficient to achieve fluoro-emulsions with higher stabilities. Such emulsions were further polymerized to obtain hierarchical porous polymers in order to use in practical applications. The first reason to explain the stability of CFS co-stabilized HIPE against conventional surfactants was the viscosity of emulsions, as it is well known that by increasing the viscosity of emulsions their stability can be increased (Ikem et al., 2008). The Second reason to explain diversity between two types of emulsion systems may be due to the presence of fluorine contents in both CFS and monomer used in the preparation of HIPEs but on the other hand, conventional surfactants were fluorine-free. Hence fluoro-compatibility of both surfactant and monomer lead towards long-term fluoroemulsion stability (Azhar et al., 2017a).

4.4. Morphology of magnetic Poly(HFBA-DVB) foams

The effect of change in concentration of CFS (by keeping HA-Fe_3O_4 concentration constant) on the morphology of magnetic polyHIPEs was investigated. A dramatic change in size and morphology of the foams was observed by changing the concentration of CFS from 3 wt% to 12 wt% as shown in Fig. 6. When the CFS concentration was low to 3 wt% the sizes of the pores were higher (23 μm) and it gradually decreased by increasing surfactant concentration to 9 wt% (4.92 μm). The reason of reduction in diameter of pores is attributed to the coalescence phenomena in which many small droplets combine together to form bigger droplets. It means that at lower surfactant concentration the coalescence in between droplets was higher, and by increasing surfactant concentrations to the certain level, coalescence also decreased which prevents the formation of bigger droplets (Perez-Garcia et al., 2016). At 12 wt% CFS concentration a regular polyHIPE structure was lost (Fig. 6d). It was due to the reason that by increasing surfactant concentration the oil layer between water droplets started thinning, then at the points where these water droplets touched each other inferred small openings in the form of pore throats. This oil layer shrank more and more by increasing CFS concentration and the process continued to increase until the level of the surfactant concentration came when this thin layer disappeared after maximum thinning. At that point, "struts" instead of regular polyHIPE morphology were obtained, which resulted in catastrophic drop in bulk physical continuity (Wrobleski, 1987). Sizes of the pores followed a declining trend by increasing

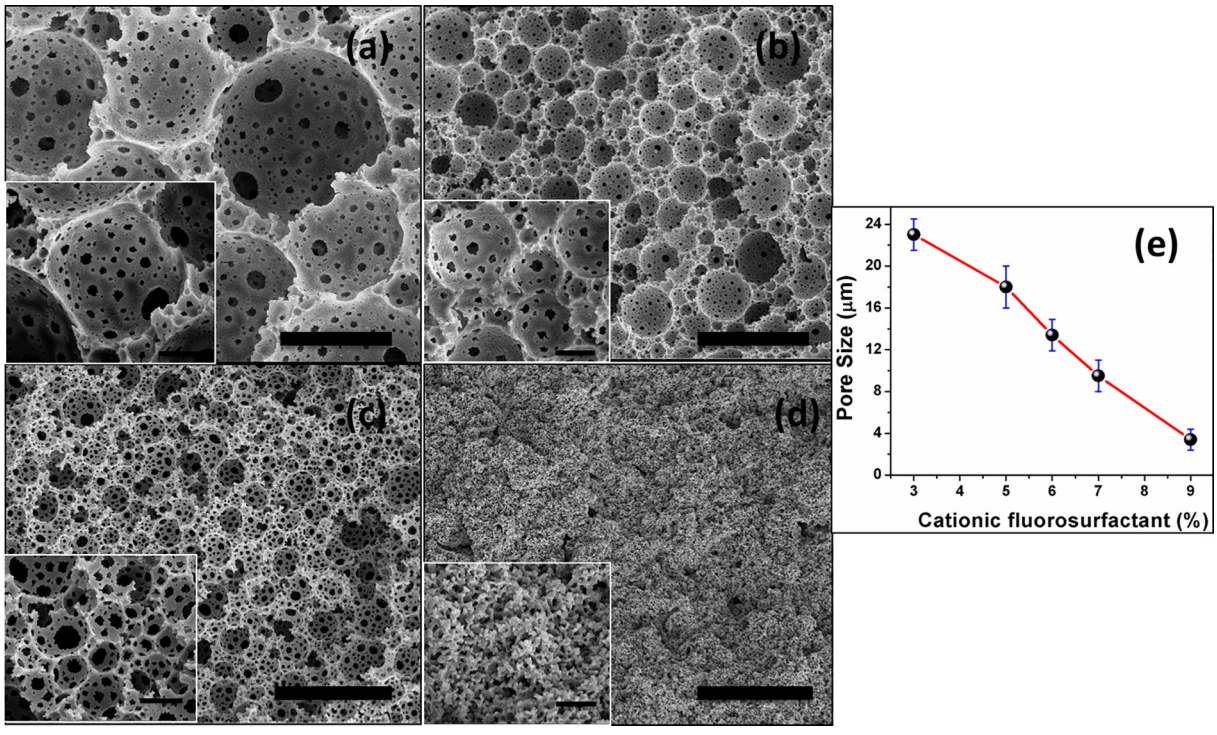

Fig. 6 Tuning the pore sizes by varying amount of surfactant in co-stabilized emulsion systems, SEM images: (a) 3 wt% (sample 1), (b) 6 wt% (sample 2), (c) 9 wt% (sample 3), (d) 12 wt% (sample 4) and (e) Effect of CFS wt% (constant NPs concentration) on pore sizes of polyHIPEs (main scale bar for SEM: 20 μm; and inset scale bar: 5 μm).

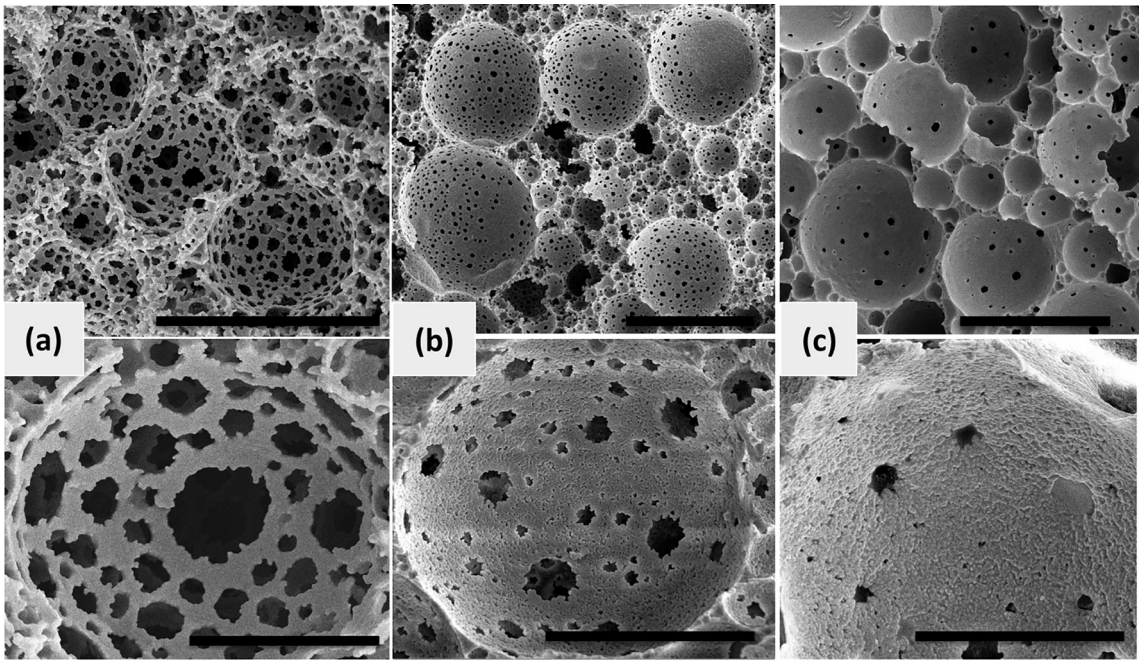

Fig. 7 Effect of HA-Fe_3O_4 concentration (constant CFS 8 wt%) on openness of polyHIPEs: (a) sample 5, (b) sample 6, and (c) sample 7; (Upper images scale bar 50 μm, Lower images scale bar 10 μm).

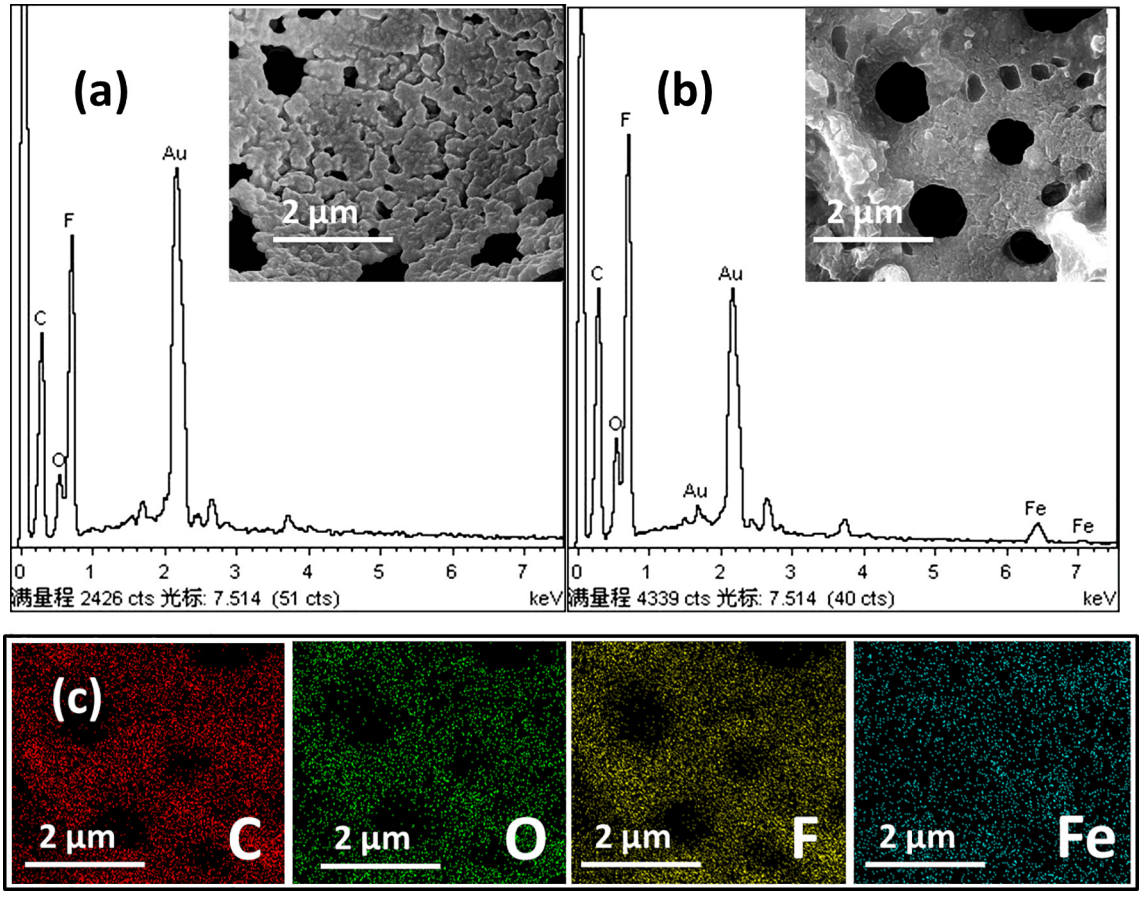

Fig. 8 EDXS analysis of with and without nanoparticles polyHIPE: (a) sample 8, and (b) sample 2; (insets are SEM images of relative samples), and (c) elemental mapping of sample 2.

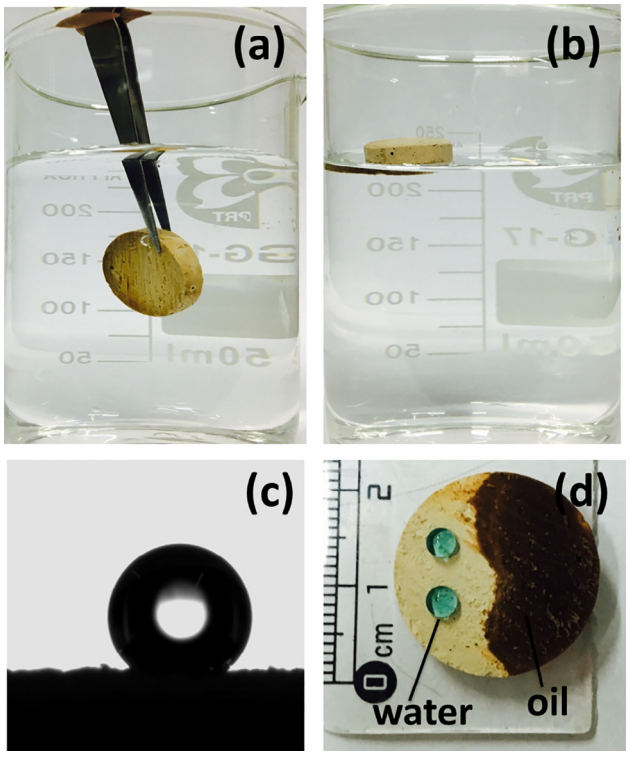

Fig. 9 Hydrophobicity and oleophilicity of magnetic poly (HFBA-DVB) foam (sample 3); (a) immersed in the water by external force, (b) floating on water surface upon releasing of external force, (c) water contact angle = 139°, and (d) water (dyed with $CuSO_4$) droplet and oil (gasoline) on the surface.

CFS concentration as shown in Fig. 6e. It shows that fluoropolymer HIPEs also followed the same trend in investigation of pore sizes as of various common organic polymer such as styrene, methyl methacrylate, etc. with respect to surfactant concentration change (Pulko and Krajnc, 2012).

Fig. 7 demonstrates SEM micrographs of magnetic polyHIPEs with variable amount of HA-Fe_3O_4 and constant CFS concentration. Higher level of openness was observed in sample 5 (Fig. 7a). Interconnectivity became lesser in sample 6 (Fig. 7b) and almost a closed cell structure was achieved in sample 7 (Fig. 7c). Here in the interconnectivity of co-stabilized system of polyHIPEs was tuned by two contradictory factors, the hindrance of HA-Fe_3O_4 NPs and volume contraction of the continuous phase caused by polymerization. At lower NPs contents, the polymerization shrinkage generated bigger pore throats in sample 5. However, the throats started to partially close in sample 6 and fully closed in sample 7 indicated the increased hindrance from the enhanced stabilizer at the water-oil interface could preponderate the strong polymerization shrinkage of monomer. It has been proven that adequate volume shrinkage of polymeric networks during polymerization process leads to the formation of open throats. However, the barrier effect of solid NPs with high content is effective to hinder the formation of pore throats (Hongyun, 2015). Decreasing openness with increasing concentration of HA-Fe_3O_4 plots are presented in (Fig. S2).

Comparison of polyHIPEs with and without nanoparticles was confirmed by Energy Dispersive X-ray Spectroscopy (EDXS) as shown in Fig. 8. There was no iron (Fe) found in the EDXS graph of the emulsion prepared without nanoparticles (Fig. 9a), but the presence of Fe in Fig. 8b verified the presence of magnetite nanoparticles in the polymer matrix. Elemental mapping of sample 2 is presented in Fig. 8c. This proved that Fe_3O_4 particles in HIPE were well dispersed in HIPE and acted as Pickering stabilizer to form magnetic polyHIPE monoliths. Au peaks in the EDXS plots were due to the gold sputtering on both samples before the analysis for better conductivity.

4.5. Oil adsorbency and magnetic ability of PolyHIPEs

The porous polymeric materials with superb hydrophobicity and oleophilicity characteristics demonstrate high oil-water separation efficiency. The foremost requirement for a sorbent material is that the surface should be composed of low surface energy components. Fluoropolymers such as poly(vinylidene fluoride) (PVDF) and poly(tetrafluoroethylene) (PTFE) provide efficient hydrophobic and oleophilic surfaces because of the low surface energy of the carbon and fluoride groups (Xiang et al., 2015; Zeng et al., 2015). In this work, the presence of highly hydrophobic fluoro atoms was seen in EDXS results of Fig. 8, which made the magnetic Poly(HFBA-DVB) foams highly hydrophobic. Also, the low density of the foams ensured floatability of the foams on the surface of the water as depicted in Fig. 9. Forceful dipping of fluoropolymer monolith in water can be seen in Fig. 9a, and when the force was removed that again floated on the water surface Fig. 9b. The water contact angle was measured to be 139°, which also showed that the prepared product was highly hydrophobic in nature (Fig. 9c) (Azhar et al., 2017b; Zhang et al., 2007). When the gasoline was dripped on the surface of the porous foam, it was immediately penetrated into the surface due to the capillarity action but water formed spherical droplets on the hydrophobic polyHIPE, as shown in Fig. 9d. Water repellency together with oil adsorption enabled the potential application of magnetic poly(HFBA-DVB) foam for water/oil separation.

Adsorption experiments for DCM, gasoline, THF and n-Hexane were carried out. Fig. 10 depicts the separation process of gasoline (dyed with Sudan II) from water, recyclability of magnetic fluoropolymers and effect of cationic fluorosurfactant concentration change on oil adsorption capacities of the fluoropolymer. As the foams were magnetic, these were easily guided on desirable areas of oil spots on water surface and promptly pulled out by handheld magnet after adsorption saturation. This characteristic could provide the material with considerable assistance during practical applications in oil spillage cleanup. Oil adsorption capacities were first increased upon raising the concentration of CFS due to more number of pores along with increased openness, and then suddenly decreased at 12 wt % CFS concentrations due to the loss of regular porous morphology of polyHIPEs at higher concentration. Magnetic polyHIPEs prepared in this study adsorbed the oil to 14 times the mass of monolith which is considerably higher than previous literature report on porous fluoropolymer without nanoparticles in which oil adsorption capacity was calculated to be less than 7.1 g/g of adsorbent (Azhar et al., 2017a).

After adsorption saturation, the oil was collected back from the polyHIPEs by means of centrifugation, and material was

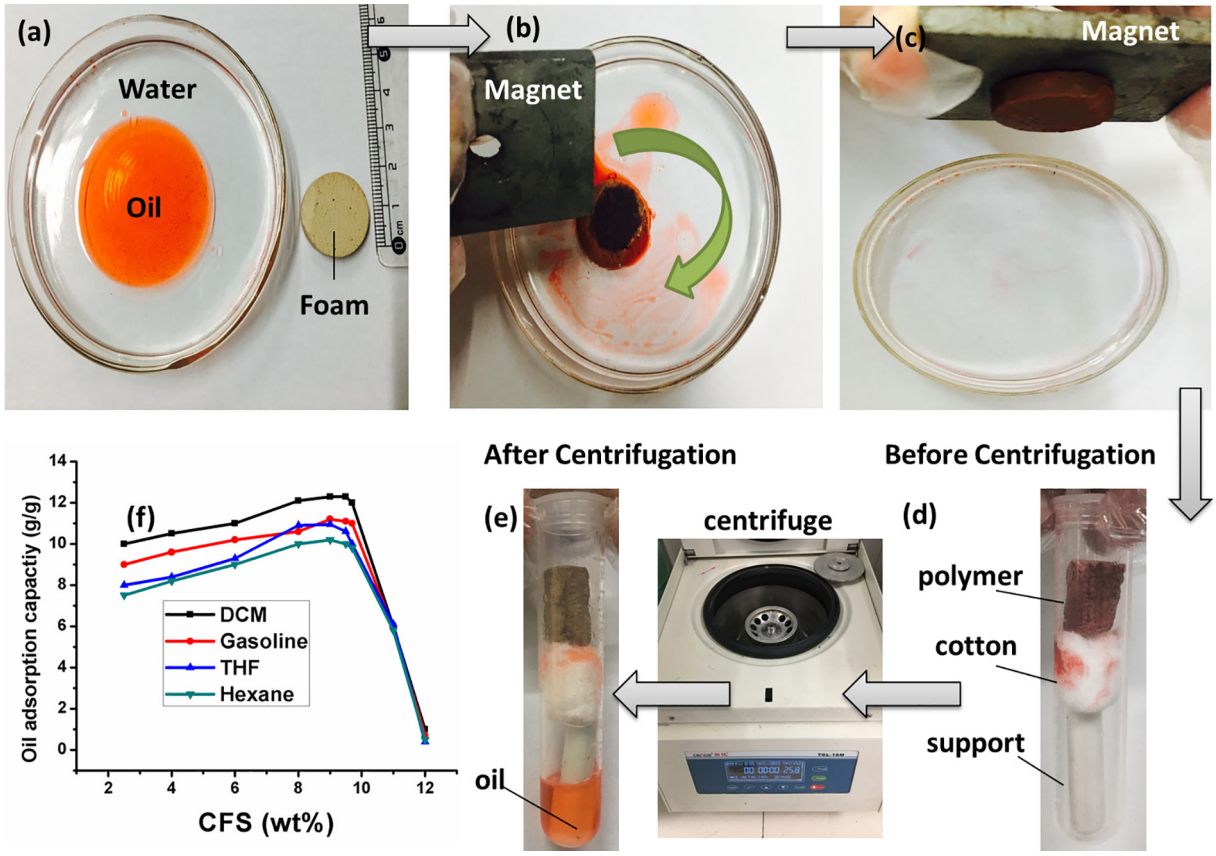

Fig. 10 Demonstration of significant application of magnetic polyHIPE (sample 3); (a–c) Oil adsorption process, (d–e) regeneration by means of centrifugation, and (f) change in oil adsorption capabilities of porous polyHIPEs by varying amount of surfactant.

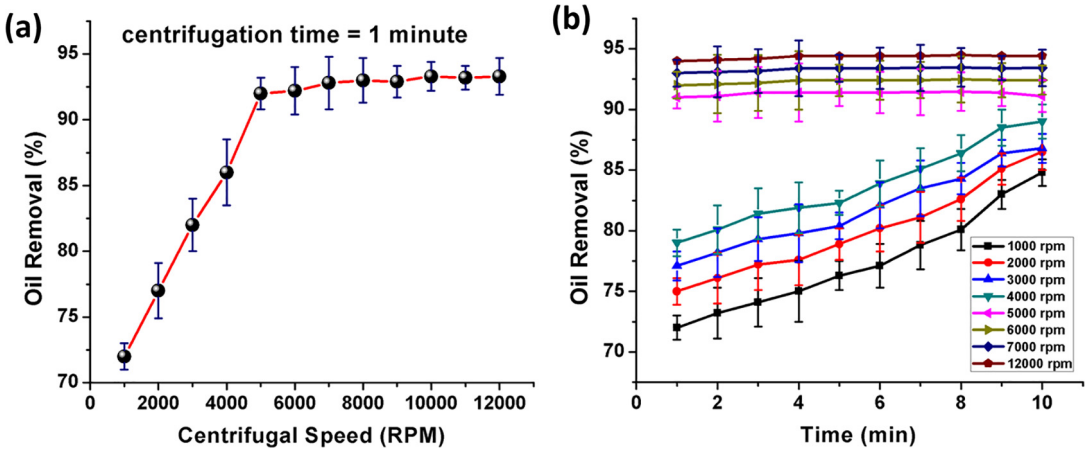

Fig. 11 Relationship between oil removal (%) and (a) centrifugal speed, (b) centrifugal time.

also regenerated at the same time (Fig. 10d, e). The polymer monolith was taken in a centrifugal tube for recycling experiments, the cotton bud supported by some solid placed in longitudinal direction (magnetic stirrer in this work). Centrifugal tube was then placed in a centrifuge for desired experimental steps. After completion of one centrifugation cycle, the foam was quickly utilized to the next cycle of oil adsorption. Even after 10 adsorption/regeneration cycles, the oil adsorption capacity was not decreased. However, after 10 cycles, the structural integrity of material was started to destroy and cracks were prominent on the surface. In each cycle (after the first cycle) the retained quantity of oil in polyHIPE was

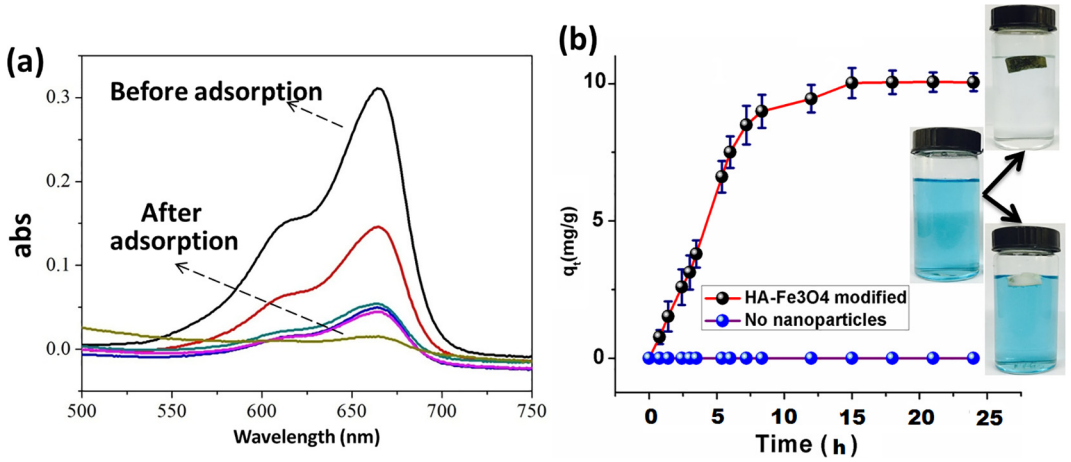

Fig. 12 Methylene blue adsorption by polyHIPEs; (a) UV–vis spectra of methylene blue dye adsorbed by functional polyHIPE composites, and (b) Adsorption kinetics curves for polyHIPEs sample 6 (red curve) and sample 8 (purple curve).

also constant at 3g/g (Zhang et al., 2016) (Fig. S3). For material regeneration efficiency, many centrifugation speeds with same centrifugal time of 1 min were measured and results are summarized in Fig. 11a. The speed of around 5000 RPM was enough to attain de-oiling rate of approximately 91%, and this seemed to be most suited. An increase of RPM from 5000 to 12,000 only resulted in a minute improvement in de-oiling rate. Fig. 11b gives information about the experimental data that elongation of time was beneficial for oil removal at lower RPM. However, > 5000 RPM only gave the straight line with no significant inclination after 1 min (Zhang et al., 2015).

The saturation magnetization, which was evaluated by vibrating sample magnetometer (VSM) was around 12 emu/g (sample 6), as shown in (Fig. S4a). It can also be seen that the value of magnetization was 0 emu/g when there were no NPs in the composite (sample 8). The digital photographs (Fig. S4b) depicts the magnetic behavior of fluoropolymer foams with and without incorporation of nanoparticles. It is clear from the figure that PolyHIPE with functional nanoparticles stuck well with the magnet but white color polyHIPE (with no nanoparticles; sample 8) remained unaffected near the handheld magnet.

4.6. Methylene blue dye adsorption

Magnetic polyHIPE foams were efficiently able to adsorb organic dyes from water. As these functional polyHIPEs possessed ionic functional groups such as carboxyl, phenolic hydroxyl, carbonyl, methoxyl, ether and amino in framework, which had superb ability to adsorb and trap ionic dyes and metal ions from water (Wang et al., 2011). Also, it has been justified in above section that humic acid was successfully coated on the surface of nanoparticles and further these nanoparticles were dispersed well in the polyHIPE matrix. A cationic dye (methylene blue) was utilized to test adsorption behavior of polyHIPEs. UV–vis curves for adsorption of dye from water are shown in Fig. 12a. Typical MB peaks at 664 nm were observed in all experiments which became lower and lower in intensity upon increasing time. Fig. 12b shows digital images (after 15 h) of adsorption of MB into two types of polyHIPEs (with and without nanoparticles). It can be seen that MB was totally eradicated from water/MB solution by the action of functional polyHIPEs (HA-Fe_3O_4 modified), on the other hand, the same blue color solution of MB was found after a given time period by treating it with non-functional polyHIPEs (without HA-Fe_3O_4. The adsorption capacity of functional monolith came out to be 10.25 mg/g, which was significantly higher than the recent report on styrene-DVB polyHIPEs for cationic dye adsorption i.e. 1.90 mg/g (Mert et al., 2017). Nonetheless, practical usage is related more to the adsorption kinetics. Fig. 12b demonstrates the adsorption kinetics of MB by both types of polyHIPEs i.e. Functional (sample 6) and simple without NPs (sample 8). It took only 15 h to achieve adsorption equilibrium by magnetic polymer while polyHIPEs prepared without nanoparticles did not adsorb MB, due to the absence of functional nanoparticles in the polymer matrix. This adsorption kinetics is also better than the cationic dye adsorbents reported by Mert et al. (2017), which took 13 days to reach kinetic equilibrium for styrene-DVB polyHIPE composites. It indicates that HA-Fe_3O_4 nanoparticles immobilized on polyHIPE matrix significantly enhanced the adsorption capacities and kinetics towards cationic dyes.

5. Conclusions

In summary, CFS and HA-Fe_3O_4 nanoparticles were prepared and used together to stabilize the fluoro-emulsions which produced highly porous functional poly(HFBA-DVB) interconnected foams. It was found that conventional surfactants combined with Fe_3O_4 to emulsify HIPE failed to stabilize fluoro-HIPEs. Hence for the first time, cationic fluorosurfactant with functional magnetite nanoparticles was employed as co-stabilizer to stabilize fluoro-HIPE. CFS and iron oxide particles were held at the oil/water interface to act as a barrier to avoid Ostwald ripening, which proved to be an effective co-stabilizer for fluoro-HIPE templates with significantly improved emulsion stability up to 96 h (Azhar et al., 2017a). Furthermore, this bi-component stabilizer system provided a new possibility to tune the micro-structures of resulting

magnetic fluoropolymer foams. The sizes of the pores were adjusted in the range of 4.9–23 μm. The materials possessed a superb hydrophobic nature with a water contact angle of 139^0 due to the presence of fluorine in structure. As a multifunctional composite, these fluoropolymers selectively adsorb organic oils with the capacity towards DCM (14 g/g of foam) and dyes (10.25 mg of MB/g of foam) from the water. Prepared fluoropolymers were guided on desired areas of contaminated water (to collect oil) and withdrawn easily by simple handheld magnet. The centrifugal speed of around 5000 RPM was proved to be optimum for recyclability of composites to attain de-oiling rate of approximately 91%. It was found that even after 10 adsorption/regeneration cycles, the oil adsorption capacity was not decreased. All these substantial properties of fluoropolymer foams will find promising applications in the fields of separation processes, porous templates for catalysts, tissue engineering and so on.

Acknowledgements

The work was supported by National Science Foundation of China [Grant No. 21675064]; Young Taishan Scholars tsqn [Grant No. 20161036]; the National Science Foundation of China [Grant No. 21304037]; the Natural Science Foundation of Shandong Province [Grant No. ZR2017ZC0529]; and the Scientific Research project of Shandong Provincial Department of Education [Grant No. J11LB02].

Conflicts of interest

Authors declare that they have no conflicts of interest regarding this manuscript.

Appendix A. Supplementary material

Supplementary data associated with this article can be found, in the online version, at https://doi.org/10.1016/j.arabjc.2018.04.003.

References

Aveyard, R., Binks, B.P., Clint, J.H., 2003. Emulsions stabilised solely by colloidal particles. Adv. Colloid Interface Sci. 100–102, 503–546.

Azhar, U., Huyan, C., Wan, X., Xu, A., Li, H., Geng, B., Zhang, S., 2017a. A cationic fluorosurfactant for fabrication of high-performance fluoropolymer foams with controllable morphology. Mater. Des. 124, 194–202.

Azhar, U., Yaqub, R., Geng, B., Zhang, S., 2017b. Data set on stability comparison of emulsions stabilized by cationic fluorosurfactant against conventional surfactants and high thermal performance of fluoropolymer foams. Data in Brief 13, 396–400.

v.J.S. Baohua Gu, Zhlhong Chen, S. Llyuan Llang, John F. McCarthyt. Adsorption and desorption of natural organic matter on iron oxide: mechanisms and models. Environ. Sci. Technol. 28 (1994) 38–48.

Brun, N., Ungureanu, S., Deleuze, H., Backov, R., 2011. Hybrid foams, colloids and beyond: from design to applications. Chem. Soc. Rev. 40, 771–788.

Cameron, N.R., 2005. High internal phase emulsion templating as a route to well-defined porous polymers. Polymer 46, 1439–1449.

Chen, P.C., Wan, L.S., Ke, B.B., Xu, Z.K., 2011. Honeycomb-patterned film segregated with phenylboronic acid for glucose sensing. Langmuir: The ACS J. Surf. Colloids 27, 12597–12605.

David, L.C., Olson, A., Hillmyer, Marc A., 2007. Templating nanoporous polymers with ordered block copolymers. Chem. Mater. 20, 869–890.

Debecker, D.P., Boissiere, C., Laurent, G., Huet, S., Eliaers, P., Sanchez, C., Backov, R., 2015. First acidic macro-mesocellular aluminosilicate monolithic foams "SiAl(HIPE)" and their catalytic properties. Chem. Commun. 51, 14018–14021.

Dhandayuthapani, B., Yoshida, Y., Maekawa, T., Kumar, D.S., 2011. Polymeric scaffolds in tissue engineering application: a review. Int. J. Polymer Sci. 2011, 1–19.

Fongang, R.T.T., Pemndje, J., Lemougna, P.N., Melo, U.C., Nanseu, C.P., Nait-Ali, B., Kamseu, E., Leonelli, C., 2015. Cleaner production of the lightweight insulating composites: microstructure, pore network and thermal conductivity. Energy Build. 107, 113–122.

Guo, J., Du, W., Gao, Y., Cao, Y., Yin, Y., 2017. Cellulose nanocrystals as water-in-oil Pickering emulsifiers via intercalative modification. Colloids and Surf. A: Physicochem. Eng. Aspects 529, 634–642.

Hongyun Xu, X.Z., Huang, Yifei, Wang, Haitao, Du, Qiangguo, 2015. Interconnected porous polymers with tunable pore throat size prepared via pickering high internal phase emulsions. Langmuir: The ACS J. Surf. Colloids 32, 38–45.

Huang, X., Wang, R., Zhao, P., Lu, G., Zhang, S., Qing, F.-L., 2005. Synthesis and characterization of novel fluoropolymers containing sulfonyl and perfluorocyclobutyl units. Polymer 46, 7590–7597.

Ikem, V.O., Menner, A., Bismarck, A., 2008. High internal phase emulsions stabilized solely by functionalized silica particles. Angew. Chem. 47, 8277–8279.

Jafari, M., Paknejad, Z., Rad, M.R., Motamedian, S.R., Eghbal, M.J., Nadjmi, N., Khojasteh, A., 2017. Polymeric scaffolds in tissue engineering: a literature review. J. Biomed. Mater. Res. B Appl. Biomater. 105, 431–459.

Jing-Fu Liu, Z.-S.Z., Jiang, Gui-Bin, 2008. Coating Fe_3O_4 magnetic nanoparticles with humic acid for high efficient removal of heavy metals in water. Environ. Sci. Technol. 42, 6949–6954.

Kawaguchi, H., 2000. Functional polymer microspheres. Prog. Polym. Sci. 25, 1171–1210.

Kimmins, S.D., Cameron, N.R., 2011. Functional porous polymers by emulsion templating: recent advances. Adv. Funct. Mater. 21, 211–225.

Lu, A.H., Schüth, F., 2006. Nanocasting: a versatile strategy for creating nanostructured porous materials. Adv. Mater. 18, 1793–1805.

J. Ma, L. Zhang, B. Geng, U. Azhar, A. Xu, A.S. Zhang. Preparation of thermo-responsive and cross-linked fluorinated nanoparticles via RAFT-mediated aqueous polymerization in nanoreactors. Molecules 22 (2017) 1–13.

McKeown, N.B., Budd, P.M., 2010. Exploitation of intrinsic microporosity in polymer-based materials. Macromolecules 43, 5163–5176.

Mert, H.H., Tekay, E., Nugay, N., Nugay, T., Şen, S., 2017. Adsorptive polyHIPE composites based on biosorbent immobilized nanoclay: effects of immobilization techniques. Polym. Eng. Sci.

Mert, E.H., Yıldırım, H., Üzümcü, A.T., Kavas, H., 2013. Synthesis and characterization of magnetic polyHIPEs with humic acid surface modified magnetic iron oxide nanoparticles. React. Funct. Polym. 73, 175–181.

Pan, J., Zeng, J., Cao, Q., Gao, H., Gen, Y., Peng, Y., Dai, X., Yan, Y., 2016. Hierarchical macro and mesoporous foams synthesized by HIPEs template and interface grafted route for simultaneous removal of λ-cyhalothrin and copper ions. Chem. Eng. J. 284, 1361–1372.

Peng, L., Qin, P., Lei, M., Zeng, Q., Song, H., Yang, J., Shao, J., Liao, B., Gu, J., 2012. Modifying Fe3O4 nanoparticles with humic acid for removal of Rhodamine B in water. J. Hazard. Mater. 209–210, 193–198.

Perez-Garcia, M.G., Gutierrez, M.C., Mota-Morales, J.D., Luna-Barcenas, G., Del Monte, F., 2016. Synthesis of biodegradable macroporous poly(l-lactide)/poly(epsilon-caprolactone) blend using oil-in-eutectic-mixture high-internal-phase emulsions as template. ACS Appl. Mater. & Interfaces 8, 16939–16949.

Pichot, R., Spyropoulos, F., Norton, I.T., 2010. O/W emulsions stabilised by both low molecular weight surfactants and colloidal particles: The effect of surfactant type and concentration. J. Colloid Interface Sci. 352, 128–135.

Pulko, I., Krajnc, P., 2012. High internal phase emulsion templating–a path to hierarchically porous functional polymers. Macromol. Rapid Commun. 33, 1731–1746.

Raffa, P., Wever, D.A., Picchioni, F., Broekhuis, A.A., 2015. Polymeric surfactants: synthesis properties, and links to applications. Chem. Rev. 115, 8504–8563.

Ruiyun Zhang, P.X.M., 1999. Poly(a-hydroxyl acids)/hydroxyapatite porous composites for bone-tissue engineering. I. Preparation and morphology. J. Biomed. Mater. Res. 44, 446–455.

Ruiz-Hernández, E., López-Noriega, A., Arcos, D., Vallet-Regí, M., 2008. Mesoporous magnetic microspheres for drug targeting. Solid State Sci. 10, 421–426.

Schacher, F., Ulbricht, M., Müller, A.H.E., 2009. Self-Supporting, double stimuli-responsive porous membranes from polystyrene-block-poly(N, N-dimethylaminoethyl methacrylate) diblock copolymers. Adv. Funct. Mater. 19, 1040–1045.

Silverstein, M.S., 2014. PolyHIPEs: recent advances in emulsion-templated porous polymers. Prog. Polym. Sci. 39, 199–234.

Sumirat, I., Ando, Y., Shimamura, S., 2006. Theoretical consideration of the effect of porosity on thermal conductivity of porous materials. J. Porous Mater. 13, 439–443.

Tebboth, M., Menner, A., Kogelbauer, A., Bismarck, A., 2014. Polymerised high internal phase emulsions for fluid separation applications. Curr. Opin. Chem. Eng. 4, 114–120.

Tian, Y., Wu, D., Jia, X., Yu, B., Zhan, S., 2011. Core-shell nanostructure of α-Fe2O3/Fe3O4: synthesis and photocatalysis for methyl orange. J. Nanomater. 2011, 1–5.

Toledo, L., Urbano, B.F., 2016. Poly(2-hydroxyethyl methacrylate)-based porous hydrogel: influence of surfactant and SiO2 nanoparticles on the morphology, swelling and thermal properties. Eur. Polym. J. 81, 316–326.

Vilchez, A., Rodriguez-Abreu, C., Menner, A., Bismarck, A., Esquena, J., 2014. Antagonistic effects between magnetite nanoparticles and a hydrophobic surfactant in highly concentrated Pickering emulsions. Langmuir: The ACS J. Surf. Colloids 30, 5064–5074.

Wan, X., Azhar, U., Wang, Y., Chen, J., Xu, A., Zhang, S., Geng, B., 2018. Highly porous and chemical resistive P(TFEMA–DVB) monolith with tunable morphology for rapid oil/water separation. RSC Adv. 8, 8355–8364.

Wang, S., Peng, X., Zhong, L., Tan, J., Jing, S., Cao, X., Chen, W., Liu, C., Sun, R., 2015. An ultralight, elastic, cost-effective, and highly recyclable superabsorbent from microfibrillated cellulose fibers for oil spillage cleanup. J. Mater. Chem. A 3, 8772–8781.

Wang, L., Zhang, J., Wang, A., 2011. Fast removal of methylene blue from aqueous solution by adsorption onto chitosan-g-poly (acrylic acid)/attapulgite composite. Desalination 266, 33–39.

Wassana Yantasee, C.L.W., Sangvanich, Thanapon, Shane Addleman, R., Carter, Timothy G., Wiacek, Robert J., Fryxell, Glen E., Timchalk, Charles, Warner, Marvin G., 2007. Removal of heavy metals from aqueous systems with thiol functionalized superparamagnetic nanoparticles. Environ. Sci. Technol. 41, 5114–5119.

Wenwen Li, J.A.Y., Matyjaszewski, Krzysztof, 2010. Dual-reactive surfactant used for synthesis of functional nanocapsules in miniemulsion. J. Am. Chem. Soc. 132, 7823–7825.

J.M.W.A.D.A. Wrobleski, Spatial distribution of the phases in water-in-oil emulsions. Open and closed microcellular foams from cross-linked polystyrene, Langmuir: The ACS J. Surf. Colloids 4 (1987) 656–662

Wu, Y., Ma, Y., Pan, J., Gu, R., Luo, J., 2017. Porous and magnetic molecularly imprinted polymers via pickering high internal phase emulsions polymerization for selective adsorption of λ-cyhalothrin. Front. Chem. 5.

Wu, D., Xu, F., Sun, B., Fu, R., He, H., Matyjaszewski, K., 2012. Design and preparation of porous polymers. Chem. Rev. 112, 3959–4015.

Xiang, J.S.Y., Wang, Y., Liu, F., Xue, L., 2015. A pH-responsive PVDF membrane with superwetting properties for the separation of oil and water. RSC Adv. 5, 23530–23539.

Xiaojuan Feng, A.J.S., Simpson, Myrna J., 2006. Investigating the role of mineral-bound humic acid in phenanthrene sorption. Environ. Sci. Technol. 40, 3260–3266.

Xu, A., Lu, Q., Huo, Z., Ma, J., Geng, B., Azhar, U., Zhang, L., Zhang, S., 2017. Synthesis of fluorinated nanoparticles via RAFT dispersion polymerization-induced self-assembly using fluorinated macro-RAFT agents in supercritical carbon dioxide. RSC Adv. 7, 51612–51620.

J.H. Yang Liu, Jiangtao Xu, Deqin Fan, Wei Tang, Yuliang Yang. Thermal decomposition of cumyl dithiobenzoate, Macromolecules 38 (2005) 10332–10335.

Yin, D., Li, B., Liu, J., Zhang, Q., 2014a. Structural diversity of multi-hollow microspheres via multiple Pickering emulsion co-stabilized by surfactant. Colloid Polym. Sci. 293, 341–347.

Yin, D., Ma, L., Liu, J., Zhang, Q., 2014a. Pickering emulsion: a novel template for microencapsulated phase change materials with polymer–silica hybrid shell. Energy 64, 575–581.

Zeng, X., Ma, Y., Wang, Y., 2015. Enhancing the low surface energy properties of polymer films with a dangling shell of fluorinated block-copolymer. Appl. Surf. Sci. 338, 190–196.

Zhang, N., Jiang, W., Wang, T., Gu, J., Zhong, S., Zhou, S., Xie, T., Fu, J., 2015. Facile preparation of magnetic poly(styrene-divinylbenzene) foam and its application as an oil absorbent. Ind. Eng. Chem. Res. 54, 11033–11039.

Zhang, B., Liu, B., Deng, X., Cao, S., Hou, X., Chen, H., 2007. A novel approach for the preparation of organic-siloxane oligomers and the creation of hydrophobic surface. Appl. Surf. Sci. 254, 452–458.

Zhang, N., Zhong, S., Zhou, X., Jiang, W., Wang, T., Fu, J., 2016. Superhydrophobic P (St-DVB) foam prepared by the high internal phase emulsion technique for oil spill recovery. Chem. Eng. J. 298, 117–124.